

# Single-species dinoflagellate cyst carbon isotope fractionation in core-top sediments: environmental controls, CO<sub>2</sub>-dependency and proxy potential

5 Joost Frieling<sup>1,‡</sup>, Linda van Roijj<sup>1</sup>, Iris Kleij<sup>1</sup>, Gert-Jan Reichart<sup>1,2</sup> & Appy Sluijs<sup>1</sup>

1. Department of Earth Sciences, Faculty of Geosciences, Utrecht University, Princetonlaan 8, 3584CB Utrecht, The Netherlands

2. NIOZ Royal Netherlands Institute for Sea Research and Utrecht University, Texel, The Netherlands

‡ now at: Department of Earth Sciences, University of Oxford, South Parks Road, Oxford, OX1 3AN, Oxford, United Kingdom

10 Correspondence to: J. Frieling ([joost.frieling@earth.ox.ac.uk](mailto:joost.frieling@earth.ox.ac.uk))

**Abstract.** Sedimentary bulk organic matter and various molecular organic components exhibit strong CO<sub>2</sub>-dependent carbon isotope fractionation relative to dissolved inorganic carbon sources. This fractionation ( $\epsilon_p$ ) has been employed as proxy for paleo- $p\text{CO}_2$ . Yet, culture experiments indicate that CO<sub>2</sub>-dependent  $\epsilon_p$  is highly specific at genus and even species level, potentially hampering the use of bulk organic matter and non-species-specific organic compounds. In recent years, significant progress has been made towards a CO<sub>2</sub> proxy using controlled growth experiments with dinoflagellate species, also showing highly species-specific  $\epsilon_p$  values. These values were, however, based on motile specimens and it remains unknown whether these relations also hold for the organic-walled resting cysts (dinocysts) produced by these dinoflagellate species in their natural environment. We here analyze dinocysts isolated from core-tops from the Atlantic Ocean and Mediterranean Sea, representing several species (*Spiniferites elongatus*, *S. (cf.) ramosus*, *S. mirabilis*, *Operculodinium centrocarpum* sensu Wall & Dale (1966) (hereafter referred to as *O. centrocarpum*) and *Impagidinium aculeatum*) using Laser ablation – nano Combustion – Gas Chromatography – Isotope Ratio Mass Spectrometry (LA/nC/GC-IRMS). We find that the dinocysts produced in the natural environment are all appreciably more <sup>13</sup>C-depleted compared to the cultured motile dinoflagellate cells, implying higher overall  $\epsilon_p$  values and, moreover, exhibit large isotope variability. Where several species could be analysed from a single location, we often record significant differences in isotopic variance and offsets in mean  $\delta^{13}\text{C}$  values between species, highlighting the importance of single-species carbon isotope analyses. The most geographically expanded dataset, based on *O. centrocarpum*, shows that  $\epsilon_p$  correlates significantly with various environmental parameters. Importantly, *O. centrocarpum* shows a CO<sub>2</sub>-dependent  $\epsilon_p$  above ~240  $\mu\text{atm } p\text{CO}_2$ . Similar to other marine autotrophs, relative insensitivity at low  $p\text{CO}_2$  is in line with active carbon concentrating mechanisms at low  $p\text{CO}_2$ , although we here cannot fully exclude that we partly underestimated  $\epsilon_p$  sensitivity at low  $p\text{CO}_2$  values due to the relatively sparse sampling in that range. Finally, we use the relation between  $\epsilon_p$  and  $p\text{CO}_2$  in *O. centrocarpum* to propose a first  $p\text{CO}_2$  proxy based on a single dinocyst species.

## 1 Introduction

Stable carbon isotope fractionation in marine autotrophs is governed for a large part by the carbon fixing enzyme RubisCO (e.g. Farquhar et al., 1989; Roeske and O'Leary, 1984), which implies most marine organic matter and therefore sedimentary marine organic matter is strongly  $^{13}\text{C}$ -depleted with respect to the dissolved inorganic carbon (DIC) source ( $\text{CO}_2(\text{aq})$ ,  $\text{HCO}_3^-$  or  $\text{CO}_3^{2-}$ ), with the stable carbon isotope composition ( $\delta^{13}\text{C}$ ) of organic matter ranging from -10 to -30‰ (Freeman and Hayes, 1992). While many groups of marine autotrophs show clear  $\text{CO}_2$ -dependent carbon isotope fractionation ( $\epsilon_p$ ), the exact relation strongly varies between marine phytoplankton groups, genera and cell morphologies (Popp et al., 1998; Boller et al., 2011, 2015; Brandenburg et al., 2022). Still, because of the assumed  $\text{CO}_2$ -dependency of RubisCO fractionation, bulk marine organic matter and more specific organic compounds of marine autotrophs (e.g. lipids biomarkers) have been proposed and applied as  $p\text{CO}_2$  proxies over the past decades (Freeman and Hayes, 1992; Naafs et al., 2016). The application of these  $p\text{CO}_2$  proxies (e.g. Bijl et al., 2010; Pagani et al., 2011; Schoon et al., 2011; Witkowski et al., 2018) has provided constraints on past atmospheric  $p\text{CO}_2$  and earth system sensitivity beyond the ice core record (e.g. Pagani et al., 2010; PALAEOSENS, 2012). However, many of the organic compounds used for  $\text{CO}_2$  reconstructions such as alkenones (e.g. Pagani, 2013), phytane (e.g. Witkowski et al., 2018), porphyrins (e.g. Freeman and Hayes, 1992) or bulk organic matter (e.g. Hayes et al., 1999) are not related to a single species, genus or even group of organisms. This implies that reconstructions based on these compounds integrates interspecific differences in  $\text{CO}_2$ -dependency, which complicates the interpretation of such proxy records. Secondly, even if specific compounds derive from a single species or genus, they intrinsically derive from a multitude of individual organisms, differing in shape and size, affecting isotopic fractionation and hence limiting the accuracy of such  $\text{CO}_2$  reconstructions.

Part of the uncertainties and biases in carbon isotope fractionation can be circumvented if the carbon isotopic fractionation of individual fossils can be analyzed. In recent years, significant progress has been made towards a  $\text{CO}_2$  proxy based on the stable carbon isotope fractionation in organic walled dinoflagellate cysts (Burkhardt et al., 1999; Hoins et al., 2015, 2016a, 2016b; Wilkes et al., 2017). A fraction (~15%) of modern dinoflagellates produces an organic resting cyst or dinocyst as an obligatory part of their lifecycle (Evitt, 1985). The organic resting cysts from autotrophic species have excellent preservation potential, are often highly oxidation-resistant (Zonneveld et al., 1997, 2019; Kodrans-Nsiah et al., 2008) and several ubiquitous extant genera and species, such as *Spiniferites* spp. and *Operculodinium centrocarpum*, have extremely long geological records (Fensome et al., 1996; Williams et al., 2004). The ecology and morphology of these long-ranging species seemingly remained unchanged for millions of years (Frieling and Sluijs, 2018). Most importantly, recent advances in methodology allow for analyses of species-specific single-cyst  $\delta^{13}\text{C}$  (van Roij et al., 2017; Sluijs et al., 2018). This presents the opportunity to quantify environmental controls on  $\epsilon_p$  of individual dinoflagellate cysts and hence species to assess the potential to obtain more accurate paleo- $p\text{CO}_2$  estimates from sedimentary records.

Controlled growth experiments across a range of  $\text{CO}_2$  levels representative for the last glacial (e.g. Barnola et al., 1987), modern and future carbon emission scenarios (Eberlein et al., 2016; Hoins et al., 2016a, 2016b, 2015; IPCC, 2014; Rost et al.,

2006; Van de Waal et al., 2013; Wilkes et al., 2017) showed species-specific  $\epsilon_p$  for multiple dinoflagellate  
65 species. From these, the species *Protoceratium reticulatum* and *Gonyaulax spinifera* (Hoins et al., 2015, 2016a, 2016b) are of  
particular interest as these produce the organic cyst species *Operculodinium centrocarpum* sensu Wall and Dale, (1966),  
hereafter referred to as *O. centrocarpum*, and *Spiniferites (cf.) ramosus*, hereafter referred to as *S. ramosus*, respectively (Head,  
1996; Zonneveld et al., 2013). These cyst species have their first occurrences in the geological records around ~60 and 130  
70 million years ago (Ma), for *O. centrocarpum* and *S. ramosus*, respectively (Williams et al., 2004), thus providing potential for  
deep-time  $p\text{CO}_2$  reconstructions.

Before  $\epsilon_p$  values based on dinocysts can be used for reconstructing  $p\text{CO}_2$ , several fundamental questions need to be addressed.  
Although  $\delta^{13}\text{C}_{\text{DIC}}$  exerts a major control on dinocyst  $\delta^{13}\text{C}$  (Sluijs et al., 2018), it remains uncertain whether the  $\text{CO}_2$  control on  
 $\epsilon_p$  of motile cells from controlled growth experiments can be translated to their cysts formed in the natural environment. In  
addition, potential offsets in  $\epsilon_p$  values between the motile cells and the cysts need to be established. This is especially important  
75 as the cell-cyst relations in carbon isotope ratios are not necessarily straightforward, because bulk biomass such as cysts  
potentially deviates in  $\delta^{13}\text{C}$  values from the various cell components and potentially not by a constant offset (e.g. Freeman,  
2001; Hayes, 2001; Pancost and Pagani, 2006; Schouten et al., 1998; Van de Waal et al., 2013; Wilkes et al., 2018).

We here present the first core-top data for single-species dinocysts to constrain the environmental controls on  $\epsilon_p$ . We focus on  
the species *O. centrocarpum* and compare this data, when possible, to several species of *Spiniferites* (*S. ramosus*, *S. mirabilis*,  
80 *S. elongatus*) and *Impagidinium aculeatum*. The established environmental relations are subsequently evaluated using simple  
models converting carbon isotope fractionation in dinocysts into  $p\text{CO}_2$  values for the surface waters.

## 2.1 Materials

The primary dataset is based on 34 core-top samples (Table 1, Figure 1), collected from the North Atlantic Ocean and  
85 Mediterranean Sea. These samples encompass a substantial natural  $p\text{CO}_2$  (aq) gradient because the rate of cooling of the North  
Atlantic Current exceeds that of  $\text{CO}_2$  uptake, whereas  $p\text{CO}_2$  in the Mediterranean is close to or slightly above equilibrium with  
the atmosphere. Sample selection is further based on the dinocyst occurrence maps of Zonneveld et al. (2013), including only  
samples with an expected relative abundance of at least 10-20% of the target species. Similarly, the coverage of environmental  
parameters such as sea surface temperature (SST) and  $p\text{CO}_2$  and difference in environmental settings was maximized during  
90 sample selection. Existing ocean databases are used for obtaining the relevant environmental parameters (Table 1).

## 2.2 Methods

Using standard palynological techniques (see e.g. Brinkhuis et al., 2003), ca. 5–10 g freeze-dried sediment of the  
upper 1-2 cm of core material was processed for each sample. This involved dissolving carbonates and silicate components  
95 using strong acids (HCl, 30% and HF, 38–40%). After acid steps, residues were pH-neutralized and sieved using an ultrasonic  
bath and 250 and 10 $\mu\text{m}$  nylon mesh sieve to remove large and small particles, respectively. Subsequently, samples were

transferred to glass test tubes with demineralized water and centrifuged at 3200 rpm for 10 minutes to obtain an optimum concentrate of the sample material. Prior to dinocyst selection, samples were stored in 4 mL glass vials in demineralized water.

100 A micro-manipulator consisting of a Leica inverted microscope and a Narishige IM-9B microinjector connected to a  
strung-out pipette was used to manually select individual dinocysts from a water droplet on a glass petri dish. Dinocyst  
selection followed a strict protocol, in which cyst morphology (primarily cyst shape and process length) was kept constant and  
contribution of other organic particles minimized. Specimens with darker coloration or amorphous organic matter adhered to  
the cyst or processes were avoided. In the case of *O. centrocarpum*, the morphological selection primarily involved selecting  
specimens of equal size and process length to avoid cysts that may be derived from different environments (e.g. Mertens et al.,  
105 2009). For *Spiniferites*, we were able to distinguish and separate three distinct morphological species in sufficient numbers; *S.*  
*ramosus*, *S. elongatus* and *S. mirabilis*. For all dinocyst species, the selected diameter excluding processes was in the order of  
~30–40  $\mu\text{m}$ , except for *S. mirabilis* (~60  $\mu\text{m}$ ), although constraining the exact size of each individual specimen was not feasible  
within the current analytical procedures. Stable carbon isotope analyses for individual samples are based on replicating the  
analyses of single of dinocysts, with ~30 individual measurements being conducted to obtain a reasonably precise (~0.3–0.4‰)  
110 sample average (van Roij et al., 2017). Given the size of the dinocysts used here (~30–40  $\mu\text{m}$  cyst diameter), 3–7 specimens  
were required for each measurement and hence ~150 cysts were required to obtain sample averages (Table 1).

Dinocysts were placed on a 6 mm  $\varnothing$  nickel sample tray, after which an identical second tray is added on top and  
compressed to fixate the dinocysts. Before placement in the ablation chamber, approximately ~1 mm<sup>2</sup> of International Atomic  
Energy Agency CH-7 (IAEA-CH7) polyethylene standard (PE; certified  $\delta^{13}\text{C}$  value -32.15‰  $\pm$  0.05‰; 1 $\sigma$ ) was added to the  
115 sample tray. Stable carbon isotope analyses of the dinocysts followed the procedures described in previous work (van Roij et  
al., 2017; Sluijs et al., 2018), utilizing the recently developed Laser Ablation – nano Combustion – Gas Chromatography –  
Isotope Ratio Mass Spectrometry (LA-nC-GC/IRMS) method. Fragments resulting from deep ultraviolet LA were carried  
using a continuous Helium flow in 0.32 mm capillaries and oxidized in a combustion oven at 940 °C. The resultant CO<sub>2</sub> was  
transported to a GC combustion interface, dried in a nafion tube using a He counterflow and subsequently into a ThermoFisher  
120 DeltaV Advantage IRMS for isotope analysis. Each analytical run included 5 standards with signal intensity above 4 Vs (ca.  
40 ng C;  $\delta^{13}\text{C}$  precision better than 0.5‰) to allow calibrating to the Vienna Peedee Belemnite (VPDB) scale. Direct visual  
monitoring of the ablation process was used as initial quality assessment of each individual measurement.

To calculate the fractionation factor  $\epsilon_p$  of the dinocysts relative to dissolved inorganic carbon (DIC) from which the  
dinocyst was produced, we take the  $\delta^{13}\text{C}_{\text{DIC}}$  from the modeled grid of Tagliabue and Bopp (2008). As many dinoflagellate  
125 species, including those that produce *O. centrocarpum* and *S. ramosus* cysts, are able to utilize both HCO<sub>3</sub><sup>-</sup>, which makes up  
the majority of DIC, and CO<sub>2</sub> for carbon fixation (Hoins et al., 2016a), we also compare the  $\delta^{13}\text{C}_{\text{DINO}}$  data to  $\delta^{13}\text{C}_{\text{CO}_2}$  and with  
overall sea water carbon partitioning.

$\epsilon_{p\text{-DIC}}$  is calculated as:  $\delta^{13}\text{C}_{\text{DIC}} - \delta^{13}\text{C}_{\text{DINO}}$  and  $\epsilon_{p\text{-CO}_2}$  is calculated as  $\delta^{13}\text{C}_{\text{CO}_2} - \delta^{13}\text{C}_{\text{DINO}}$ . For the latter the  $\delta^{13}\text{C}$  of  
dissolved CO<sub>2</sub> is calculated from  $\delta^{13}\text{C}_{\text{DIC}}$  using the temperature-dependent fractionation between DIC and CO<sub>2(aq)}</sub> (Mook et  
130 al., 1974). To evaluate the dominant contributions to <sup>13</sup>C-fractionation in dinocysts, we compare the  $\epsilon_{p\text{-DIC}}$  and  $\epsilon_{p\text{-CO}_2}$  values to

measured and interpolated physicochemical parameters. We test a suite of parameters,  $[\text{NO}_3^-]$ ,  $[\text{PO}_4^{3-}]$ ,  $[\text{Si}]$ , alkalinity,  $p\text{CO}_2$ , SST and SSS, which are extracted using Ocean Data Viewer (<https://data.unep-wcmc.org/>) from existing (gridded) datasets (Gouretski and Koltermann, 2004; Takahashi et al., 2014, 2016) (Supplementary Data File). Where possible, data are averaged over a grid  $4^\circ$  longitude and latitude around the sample position. This is both to reduce errors introduced by data scarcity and to account for potential lateral transport of dinocysts during sinking (Nooteboom et al., 2019). Carbonate chemistry is calculated using the R-package *seacarb* (Gattuso et al., 2019), with alkalinity and  $p\text{CO}_2$  as input variables to calculate the other relevant parameters of the carbonate system: the relative contributions of  $\text{CO}_2(\text{aq})$ ,  $\text{HCO}_3^-$  and  $\text{CO}_3^{2-}$ , i.e. carbon speciation.

Ideally, all environmental parameters would be known for the different locations, as well as the time the dinoflagellates lived and encysted. This is, however, unfeasible because the dinocysts assemblage in core-top sediments (typically the upper 2 cm of sediment) integrates conditions over several centuries, assuming moderate to low average sediment accumulation rates ( $< 10 \text{ cm kyr}^{-1}$ ). We therefore apply a rough correction for  $p\text{CO}_2$ , based on the assumption that local air-sea gas exchange has remained similar, that equals the atmospheric  $p\text{CO}_2$  rise between the sampling date and 1850 CE. While the correction from actual measurements to ‘pre-industrial’ conditions for  $p\text{CO}_2$  is substantial due to the  $\sim 90$  ppmv atmospheric  $p\text{CO}_2$  rise from 1850 CE to *ca.* 2000 CE, this correction has only a small impact on the patterns in the  $\text{CO}_2$  data (Supplementary Figure S1). Changes in SST, SSS and nutrient concentrations are also expected, partly also by anthropogenic activity, but offsets in these parameters are generally subtle and more local compared to the changes in  $p\text{CO}_2$  and hence would require site-specific reconstructions. Still, recent wide-spread eutrophication and enhanced productivity may impact the carbon isotope results through increased DIC uptake in algal blooms (i.e. counteracting the impact of enhanced  $p\text{CO}_2$ ). However, as eutrophication mainly affected coastal areas (Hallegraeff, 1993; Anderson et al., 2002), this is expected to play a minor factor at our, mostly open marine, sample localities (Figure 1). Lastly, long-term natural changes in nutrients, SSS and SST also occur, and it is currently not possible to fully filter out the various anthropogenic offsets. With the exception of  $p\text{CO}_2$ , we hence assume all parameters (SST, SSS, nutrients) to have remained constant over the period the core top samples represent.

### 3. Results

#### 3.1 Carbon yields from dinocyst analyses

Despite our pre-screening to include only samples with high relative abundances of the target species, some of the selected samples contained too few dinocysts or in too low abundance relative to other organic particles (amorphous organic matter, plant debris, pollen, non-dinocyst marine palynomorphs etc.), to be used in our study. Ultimately, out of the initial sample set of 34 samples, 19 were found suitable for species specific dinocyst stable carbon isotope analyses (Table 1).

Typically,  $\sim 150$  individual cysts were picked and analyzed for a total of 20–50 measurements, amounting to 3–7 cysts per carbon isotope measurement. We calculate an average signal size of 0.2 Vs for a single cyst, which amounts to a carbon yield of  $\sim 6\text{--}7 \text{ ng C cyst}^{-1}$  (van Roij et al., 2017). Although the variability in signal intensity from individual measurements suggests there is substantial intra-sample (cyst-cyst) variability, no significant offsets in average carbon content per cyst were observed

165 between samples, suggesting the average carbon content of the cysts within each of the analyzed populations is similar. *Spiniferites mirabilis* is the notable exception to this rule, as far fewer specimens of this species are needed for a single  $\delta^{13}\text{C}_{\text{cyst}}$  measurement. Based on the signal intensity per specimen we estimate that this larger cyst species contains twice the amount of C compared to *S. ramosus*, *S. elongatus* and *O. centrocarpum*.

## 170 **3.2 Carbon isotope data**

### 3.2.1 Signal Intensity

The 949 individual analyses range in  $\delta^{13}\text{C}$  from  $\sim -18.5\text{‰}$  to  $-35.5\text{‰}$ . No relation was observed between  $\delta^{13}\text{C}$  and signal size (Vs), except at the very low end ( $\leq 0.2$  Vs) (Figure 2), in line with earlier analyses (van Roij et al., 2017). In this low range, the median of the  $\delta^{13}\text{C}$  values rises from  $-28\text{‰}$  below 0.1 Vs to values between  $-22$  and  $-25\text{‰}$  above 0.2 Vs. In the  $\leq 0.2$  Vs range  
175 the  $\delta^{13}\text{C}$  average of both the cysts and PE converge between  $-25\text{‰}$  and  $-30\text{‰}$ , with substantial scatter. Poorer performance at such low C masses and signal intensities is expected, as these extremely small signal sizes and poor signal to noise ratio (below  $\sim 3:1$ ) approach the limit of our method. Consequently, even a very minor contamination source would bias values and result in larger scatter, as also apparent in the PE standard at a similar signal intensity (van Roij et al., 2017; Figure 2). Due to a worsening signal-noise ratio, we find a noticeable degree of  $\delta^{13}\text{C}$  biasing from a background C source within the system is  
180 likely to occur at signal intensities  $\leq 0.5$  Vs and are particularly pronounced  $\leq 0.2$  Vs, and values for the standard and dinocysts converge around  $-27\text{‰}$  in this range (Fig. 2A). A similar background  $\delta^{13}\text{C}$  value was also obtained after liquid nitrogen trapping (van Roij et al., 2017). The source of this C remains elusive. It is unlikely to be related to the ablation (etching) of the nickel plate or associated with the water used to pick sample from, as measured blanks for those result in much lower signal intensities and neither source would affect the measurements of the PE standard. Lastly, a significant contribution of  
185 atmospheric  $\text{CO}_2$  ( $\delta^{13}\text{C}$  around  $-8\text{‰}$ ) appears unlikely due to the  $\delta^{13}\text{C}$  signature of the background signal ( $-27\text{‰}$ ). Though the origin of the background C remains unknown, we can use the trapping experiment to estimate the relevant background contribution (van Roij et al., 2017). We calculate the typical contribution is likely between 0.024 and 0.08 Vs, given a background C flux of 0.0008 Vs per second (van Roij et al., 2017) and typical duration of measurements (30–50 s for  $\delta^{13}\text{C}_{\text{DINO}}$  and up to  $\sim 100$  s for PE standard).

190 Before comparing our data with environmental variables, we therefore assess the impact of a very minor, but consistent, background contamination on the carbon isotope signal at low signal intensities (e.g. Fig. 2A). We find that a constant addition of *ca.* 0.04 Vs ( $\leq 1$  ng C) of a background C source with a  $\delta^{13}\text{C}$  of  $-27\text{‰}$  can explain the positive skewing in the standard PE  $\delta^{13}\text{C}$ . Using a simple isotope endmember / mass balance mixing model to correct for skewing (Fig. 2B), we calculated an average deviation from the measured PE and dinocyst values for intensities below 0.2 Vs in the order of  $|2.6\text{‰}|$  and  $|1.3\text{‰}|$ ,  
195 respectively. The standard deviation of the data increases approximately 3-fold (Figure 2B) compared to the raw measurement data below 0.2 Vs, but remains virtually unchanged above 0.2 Vs and the calculated deviation from the measured value is also much reduced above 0.2 Vs ( $< 0.3\text{‰}$ ).

The data correction using our simple mixing model eliminates the skew towards -27 ‰ at low signal intensities, and removes signal size  $\delta^{13}\text{C}$ -dependency below 0.2 Vs for both the isotopically homogeneous PE and the heterogeneous dinocyst data (Figure 2A, B). This suggests our method of bias correction is warranted, but the increased variability at very low intensities and lack of independent control on the exact size and  $\delta^{13}\text{C}$  of the background contamination implies the data associated with the lowest signal intensities remain significantly less reliable. We therefore apply a conservative cut-off, and use only corrected data with a signal size above 0.2 Vs.

### 3.2.2 Outlier analysis

The drift-corrected  $\delta^{13}\text{C}_{\text{DINO}}$  is non-normally distributed in many samples and also in different species (Table 1, Figure 3). Distributions tend to be tailed towards lower values. This is not due to analytical error or otherwise related to low signal intensity as we used a 0.2 Vs cut-off to eliminate samples with potentially unreliable signal-noise ratios (see above) and a minor correction for background C addition was sufficient to eliminate skewing at low signal intensities. The remainder of skewing in the sampled populations thus represents a real signal.

As age integration in the modern era may result in a mixture of cysts representing a range of environmental conditions, especially with respect to  $\text{CO}_2$  concentrations and  $\delta^{13}\text{C}_{\text{DIC}}$ , it is important to consider the potential age-distribution of dinocysts before comparing  $\delta^{13}\text{C}_{\text{DINO}}$  and  $\epsilon_p$  to environmental variables. In an ideal scenario, cysts produced after 1850 CE should be avoided in proxy-calibration efforts to eliminate a systematic bias towards the most recent times when atmospheric  $\text{CO}_2$  was already elevated above pre-industrial Holocene background (~280 ppmv). Based on typical deep ocean sedimentation rates in the range of centimetres per kyr, the core-top samples are expected to contain a mixed assemblage of dinocysts produced mostly within the last centuries to millennia but also includes cysts produced during the last few decades that are likely affected by anthropogenic influences. Including recent cysts could skew  $\delta^{13}\text{C}_{\text{DINO}}$  towards lower values through a combination of the influence of fossil fuel combustion on the  $\delta^{13}\text{C}$  of atmospheric and surface ocean  $\text{CO}_2$  (Suess-effect; Francey et al., 1999; Keeling et al., 2017) and enhanced carbon isotope fractionation at higher  $p\text{CO}_2$  in photoautotrophs, including dinoflagellates (Freeman and Hayes, 1992; Pagani, 2013; Hoins et al., 2015). This is particularly relevant for cysts formed after 1950 common era (CE), as that period accounts for most of the  $p\text{CO}_2$  rise (>130 ppmv since 1850 CE, of which >100 ppmv after 1950 CE) and  $\delta^{13}\text{C}$  decrease (~2‰ since 1850 CE of which >1.5‰ occurs after 1950 CE) (Francey et al., 1999; Keeling et al., 2017). Unfortunately, an accurate age-correction for the Suess-effect is technically unfeasible because the age-distribution of  $\delta^{13}\text{C}_{\text{DINO}}$  measurements cannot be constrained.

Instead, we therefore illustrate the influence of  $\delta^{13}\text{C}_{\text{DINO}}$  data treatment and  $p\text{CO}_2$  correction (Supplementary Figure 1). For this, we compared both measured  $p\text{CO}_2$  and  $p\text{CO}_2$  around 1850 CE (see section 2.2) to  $\epsilon_p$  calculated using both our raw  $\delta^{13}\text{C}_{\text{DINO}}$  data and the  $\delta^{13}\text{C}_{\text{DINO}}$  data after drift-correction and removal of statistical outliers identified within the sample-specific single species populations. This final step of data-treatment removed positive and negative measurement outliers from the  $\delta^{13}\text{C}$  population (outside  $\pm 2.5$  IQR), after eliminating the extremely low-signal intensities (<0.2 Vs) and correcting for the drift induced by background C in the system.

Altogether, out of a 949 measurements, we omit 43 measurements with signals  $< 0.2$  Vs and 24 statistical outliers, which leaves 882 individual  $\delta^{13}\text{C}_{\text{DINO}}$  measurements, 560 for *O. centrocarpum*, 293 for *Spiniferites* (158 *S. ramosus*, 69 *S. elongatus* and 66 *S. mirabilis*) and 29 for *I. aculeatum* (Table 1). Most of the 67 omitted measurements have comparatively low  $\delta^{13}\text{C}$  and the resulting  $\delta^{13}\text{C}$  of the populations are close to statistically indistinguishable from a normal distribution (Shapiro-Wilk  $p = 0.05\text{--}0.1$ ) or representative of a normal distribution (Table 1). Although the data-treatment partly removed the negative skew on the  $\delta^{13}\text{C}_{\text{DINO}}$  distribution (Table 1), the effects of drift-correction and outlier-removal on sample / species-mean  $\delta^{13}\text{C}_{\text{DINO}}$  are generally small (Supplementary Figure 1). This is expected as drift-correction averages only  $\sim 0.25$  ‰ and the negative and positive outliers represent only a small percentage of the total measurements (Table 1).

Distinctly non-normally distributed  $\delta^{13}\text{C}$  values were not previously observed in recent pollen and ancient dinocyst species analyzed with the same method (van Roij et al., 2016; Sluijs et al., 2018). Therefore, an influence of Suess-effect and increased  $p\text{CO}_2$  impacts on the  $\delta^{13}\text{C}_{\text{DINO}}$  data is the most likely factor to explain the predominance of  $^{13}\text{C}$ -depleted outliers and the (subtle) negative skewing of the  $\delta^{13}\text{C}$  distributions (Figure 3). Consequently, as drift-correction and outlier omission removed most of the negative skew in  $\delta^{13}\text{C}_{\text{DINO}}$  populations, this approach may have inadvertently eliminated the most severe impact of the Suess-effect. We subsequently use the background and outlier-corrected  $\delta^{13}\text{C}_{\text{DINO}}$  data and compare these data with  $\text{CO}_2$  conditions prevalent around 1850 CE. For practical purposes, we assume all populations to be normally distributed for further statistical analyses. We then use the mean carbon isotope value ( $\delta^{13}\text{C}_{\text{DINO}}$ ) and signal intensity in volt seconds (Vs) of each sample. The standard error of the mean ranges from  $\sim 0.2$  to  $0.7$  ‰ and depends primarily on the number of measurements in cases where  $n < 30$ , in line with expected values based on replicate measurements of the PE standard (van Roij et al. 2017) (Figure 4).

### 3.3 Environmental parameters and correlation

The range of measured  $\delta^{13}\text{C}_{\text{DINO}}$  values ( $\sim 5$  ‰) far exceeds the variability in surface ocean  $\delta^{13}\text{C}_{\text{DIC}}$  ( $\sim 1$  ‰) and  $\delta^{13}\text{C}_{\text{CO}_2}$  ( $\sim 2.5$  ‰), implying the observed range likely reflects differences in fractionation related to changing uptake or leakage of different inorganic carbon phases ( $\text{CO}_2$  and  $\text{HCO}_3^-$ ; Sharkey and Berry, 1985; Hoins et al., 2016a), and this hence determines most of the variability in the  $\delta^{13}\text{C}_{\text{DINO}}$  data. Here, we quantitatively assess fractionation as a function of several environmental parameters.

The simple (non-weighted) linear regressions show poor correlations between  $\epsilon_{\text{p-DIC}}$  and  $\delta^{13}\text{C}_{\text{DIC}}$  for all environmental parameters, and the correlations slightly improve when compared to  $\epsilon_{\text{p-CO}_2}$  (Table 2a, b). However, none of the tested parameters individually explain the majority of the observed variance in  $\epsilon_{\text{p-DIC}}$  (maximum  $R^2$  ( $\sim 0.1$ )) or  $\epsilon_{\text{p-CO}_2}$  (maximum  $R^2$  with  $p\text{CO}_2$  ( $\sim 0.38$ )), despite high significance (low p-values) of the regressions. The explained variance increases when polynomial regressions are applied. Several controlled growth experiments indeed show a non-linear response of  $\epsilon_{\text{p}}$  as a function of  $p\text{CO}_2$  of the growth medium (Hoins et al., 2015) although the number of data points in such experiments limit full



mathematical descriptions of the trends within the  $p\text{CO}_2$  range of this field study. Here, a second-order polynomial (quadratic) regression achieves an  $R^2$  of  $\sim 0.74$  and  $\sim 0.79$  for the non-weighted and weighted versions, respectively.

It is conceivable that other environmental parameters also significantly contribute to  $\epsilon_p$  variability (Fig. 5). For example,  $[\text{PO}_4^{3-}]$ ,  $[\text{NO}_3]$ , and  $p\text{CO}_2$  contribute significantly to a (linear) multiple-regression model, which takes the form of  $\epsilon_{p\text{-CO}_2} = c + x\text{CO}_2 + y\text{PO}_4 + z\text{NO}_3$ , where  $c$ ,  $x$ ,  $y$  and  $z$  are numerical constants. The multiple regression model using these three parameters covers  $\sim 58\%$  of the variance in *O. centrocarpum*  $\epsilon_{p\text{-CO}_2}$  (not weighted), and  $67\%$  when weighted to number of measurements per sample. Including more parameters, such as SST, oxygen concentrations, or other carbonate system parameters, explains slightly more of the observed variance, but does not significantly improve the model. The residual mean standard error (RSME) of the CNP- $\epsilon_p$  multiple regression model is  $\sim 1.45\%$  while a linear regression with only  $p\text{CO}_2$  yields  $1.7\%$ . Only weighted regressions are given here and reported ranges of the constants represent one standard error. These models have the following optimal formats:

275

Equation 1 linear:

$$\epsilon_{p\text{-CO}_2} = 6.6 \pm 2.1 + 0.031 \pm 0.008 p\text{CO}_2$$

(Adjusted  $R^2 = 0.48$ ,  $p = 0.001$ , RSME =  $1.7\%$ ) (Figure 5 a)

280 Equation 2 quadratic (only suitable for use  $> 240 \mu\text{atm}$ )

$$\epsilon_{p\text{-CO}_2} = 40.8 \pm 7.2 - 0.23 \pm 0.055 p\text{CO}_2 + 4.88 \times 10^{-4} \pm 1 \times 10^{-4} p\text{CO}_2^2$$

(Adjusted  $R^2 = 0.79$ ,  $p < 0.001$ , RSME =  $1.13\%$ ) (Figure 5 a,e)

Equation 3a multiple-regression linear:

285 
$$\epsilon_{p\text{-CO}_2} = 6.0 \pm 3.1 + 0.034 \pm 0.01 p\text{CO}_2 + 1.22 \pm 0.47 \text{NO}_3 - 10.85 \pm 3.7 \text{PO}_4^{3-}.$$

(Adjusted  $R^2 = 0.67$ ,  $p < 0.001$ , RSME =  $1.45\%$ ) (Figure 5 d)

Equation 3b adjusted for application in the paleo-domain:

$$\epsilon_{p\text{-CO}_2} = 6.0 \pm 3.1 + 0.034 \pm 0.01 p\text{CO}_2 - 1.1 \pm 5.3 \text{PO}_4^{3-}.$$

290

Equation 4 multiple-regression linear:

$$\epsilon_{p\text{-DIC}} = 18.4 \pm 3.1 + 0.025 \pm 0.01 p\text{CO}_2 + 1.45 \pm 0.47 \text{NO}_3 - 11.1 \pm 3.7 \text{PO}_4^{3-}$$

(Adjusted  $R^2 = 0.52$ ,  $p = 0.01$ , RSME =  $1.44\%$ )

295 The two linear multiple regression models are offset (Equations 3a and 4), primarily because of the carbon isotope fractionation between  $\text{HCO}_3^-$  and  $\text{CO}_2$ . The slope with respect to  $p\text{CO}_2$  also varies slightly between the models for  $\epsilon_{p\text{-DIC}}$  and  $\epsilon_{p\text{-CO}_2}$  due to

the temperature dependent fractionation between  $\text{HCO}_3^-$  and  $\text{CO}_2$ , but the slopes with  $\text{NO}_3^-$  and  $\text{PO}_4^{3-}$  are indistinguishable. The quadratic regression seemingly better fits the variability observed in  $\epsilon_{p\text{-CO}_2}$  compared to other (multiple) linear regressions and removes any structure in the residuals, potentially signaling a non-linear response in  $\epsilon_{p\text{-CO}_2}$  to  $p\text{CO}_2$ . The quadratic regression also indicates insensitivity to  $p\text{CO}_2 \leq 240 \mu\text{atm}$  and should not be used below this value (Figure 5a). When comparing  $\epsilon_p$  to  $\text{CO}_2$  around the time of measurement rather than  $\text{CO}_2$  around 1850 CE, the regression constant (intercept) shifts to accommodate the higher  $\text{CO}_2$  values but the slopes of the regressions are statistically indistinguishable (Supplementary Figure 1).

## 305 4. Discussion

### 4.1 Absolute values, comparison to marine organic matter

The recorded  $\delta^{13}\text{C}_{\text{DINO}}$  range and absolute values ( $\sim -18\text{‰}$  to  $-35\text{‰}$ ) correspond well with global  $\delta^{13}\text{C}$  values previously reported for marine particulate organic matter ( $\delta^{13}\text{C}_{\text{POC}}$ ) (e.g. (Freeman and Hayes, 1992; Goericke and Fry, 1994) and modelled phytoplankton biomass (e.g. Magozzi et al., 2017; Tagliabue and Bopp, 2008). Consequently,  $\epsilon_{p\text{-DIC}}$  and  $\epsilon_{p\text{-CO}_2}$  are also within the expected range for general marine particulate organic matter. However, the intra-sample variance of  $\delta^{13}\text{C}_{\text{DINO}}$  appears to be substantial, often spanning most of the full range ( $\sim 10\text{‰}$ ) observed for  $\delta^{13}\text{C}_{\text{POC}}$ . Some of the observed variability might be related to the limited analytical precision during measurements of the extremely small amounts of carbon of individual dinocysts. Fully constraining the contribution of this analytical uncertainty to the observed variance is, however, not possible because of unresolvable micrometer-scale heterogeneity in the PE standard (van Roij et al., 2017; Sluijs et al., 2018). In most cases, the variance in  $\delta^{13}\text{C}_{\text{DINO}}$  is similar to that of the standard. Still, it is likely that some of the seasonal  $\delta^{13}\text{C}_{\text{DIC}}$  differences are also recorded in the  $\delta^{13}\text{C}_{\text{DINO}}$ , and that some additional inter-specimen  $\delta^{13}\text{C}$  variance is present. This is to be expected since the  $\delta^{13}\text{C}$  populations from our integrated core-top samples span seasons, decades and thus also considerable variability in seawater properties and population change. In addition, growth-induced randomness and changes in  $\delta^{13}\text{C}$  and DIC in the cell's microenvironment likely contributed to inter-specimen variability. Note that in our data inter-specimen variability is still underestimated because we analyzed 3-7 specimens per ablation event, as single-cyst carbon yield ( $\sim 7 \text{ ng C}$ ) from these cyst-sizes approached the limit for reliable measurements (van Roij et al., 2016). We minimized potential influence of differences in cell size or shape through manual selection. We thus analyzed a population where the pre-selection of similar-sized cysts restricts the variance in cell surface area and volume, unlike biomarker-based proxies for which the cell size has to be reconstructed independently (Henderiks and Pagani, 2007; Stoll et al., 2019). This approach could reduce scatter in the relation of  $\epsilon_p$  to environmental variables (Popp et al., 1998).

### 4.2 Cell – cyst offset

One of the striking differences between the here generated data and the existing culture experiments, is that carbon isotope fractionation of dinocysts in the natural environment appears to be much larger than that of motile cells from controlled growth

330 (dilute batch) experiments (Hoins et al., 2015, 2016b). We find average  $\epsilon_p$  values ranging between 13–20‰ and 23–29‰ with  
respect to CO<sub>2</sub> and DIC. Cultured cells of *O. centrocarpum* yielded not only a smaller overall  $\epsilon_p$ , but also a smaller range (~8–  
12 and 18.5–20‰) across a larger CO<sub>2</sub> gradient, implying the cysts have a much steeper fractionation slope with CO<sub>2</sub> compared  
to the motile cells. Despite these differences, the average  $\epsilon_p$  for *Spiniferites* species (*S. ramosus*, *elongatus* & *mirabilis*) is often  
somewhat larger than for *O. centrocarpum* (Figure 3). This is consistent with culture experiments that showed larger CO<sub>2</sub>-  
335 dependency and overall slightly larger  $\epsilon_p$  in the motile species *G. spinifera* compared to *P. reticulatum* (Hoins et al., 2015).  
While the cultured single strains and dinoflagellate populations in nature may behave somewhat differently, we do not expect  
that this alone underlies such a marked offset between the motile cultured cells and natural cysts. Natural cysts and cultured  
cells seem consistently offset in  $\delta^{13}\text{C}$ , although at present the exact amplitude of this offset cannot be determined. However,  
such an offset is in line with certain compounds in dinoflagellate cells being depleted in  $^{13}\text{C}$  relative to the bulk biomass  
340 (Schouten et al., 1998; Wilkes et al., 2017). The organic-walled dinocysts consist of mostly aliphatic and aromatic compounds,  
forming a complex biopolymer referred to as dinosporin (de Leeuw et al., 2006; Versteegh et al., 2007, 2012). Depending on  
the biosynthetic pathway of the cyst-material and the derivation or degradation of the original compounds, this may result in  
offsets in  $\delta^{13}\text{C}$  values between cysts and the motile cells. A potential additional fractionation might be introduced during  
taphonomy and also later by the processing of sediments to concentrate the dinocysts from sediment samples. The sediment  
345 processing involves hydrochloric and hydrofluoric acids, which affects the more labile organic compounds. Last, it is  
conceivable that fractionation in the dilute batch experiments may be reduced by e.g. higher-than-natural growth rates. This  
may be supported by chemostat culture experiments on *Alexandrium tamarense* (Wilkes et al., 2017), which show a (much)  
greater fractionation compared to the dilute batch experiments (Hoins et al., 2015). However, the enhanced fractionation  
recorded in chemostat experiments is likely an artifact of isotope equilibration times exceeding CO<sub>2</sub> uptake rates (Brandenburg  
350 et al., 2022; Zhang et al., 2022). The range of options cannot be narrowed down until cultured cysts are compared to their  
motile cells harvested from the same culture, and treated with similar techniques as used for the sediments. Until these data  
become available, inferences on the origin and amplitude of the offsets between the cells and cysts of *O. centrocarpum* and  
*Spiniferites* remain speculative.

### 355 4.3 Environmental controls on carbon isotope fractionation

Carbon isotope fractionation is determined by RubisCO and several environmental parameters, dominantly  $p\text{CO}_2$ , but also cell  
size and shape, growth rates and nutrient or light regimes (e.g. Freeman and Hayes, 1992; Pagani, 2013; Popp et al., 1998;  
Stoll et al., 2019 and many others). In most cases, fractionation is  $p\text{CO}_2$  dependent, and consequently  $\epsilon_p$  in various groups and  
genera has been used as a paleo- $p\text{CO}_2$  proxy (e.g., Freeman and Hayes, 1992; Pagani, 2013; Rae et al., 2021). We performed  
360 a broad-spectrum multiple regression analysis to identify environmental factors that contribute significantly to dinocyst  $\epsilon_p$ .  
The most important parameter is  $p\text{CO}_2$ , in line with previous studies (Freeman and Hayes, 1992). A large part of the remaining  
variability can be attributed to growth rate and ultimately nutrient content, specifically nitrate and phosphate of the surface

waters, in line with previous studies on phytoplankton and dinoflagellate carbon isotope fractionation (Popp et al., 1998; Hoins et al., 2016b; Wilkes et al., 2017; Wilkes and Pearson, 2019). We find that  $p\text{CO}_2$  and  $\epsilon_p$  are positively correlated, while  $\text{NO}_3^-$  and  $\text{PO}_4^{3-}$  are negatively correlated with  $\epsilon_p$  (Fig 4).

The inclusion of nutrient levels as environmental factors on the carbon isotope fractionation reduces the error in the fit between the measured and modelled fractionation. In the rare cases where paleo-nutrient concentrations are estimated, reconstructions usually cover only  $[\text{PO}_4^{3-}]$ , implying the  $[\text{NO}_3^-]$  in Eq. 3a and 4 has to be approximated from  $[\text{PO}_4^{3-}]$ . As  $[\text{PO}_4^{3-}]$  and  $[\text{NO}_3^-]$  are generally well-correlated (typically  $\sim 1:10$   $[\text{PO}_4^{3-}]:[\text{NO}_3^-]$ ; here  $\sim 1:8$ ) in ocean waters, this is relatively straightforward. For application in the paleo-domain however, nutrient ( $[\text{PO}_4^{3-}]$ ) reconstructions may not be available or considered too unreliable to provide meaningful constraints. In specific cases where accurate paleo- $[\text{PO}_4]$  estimates or large changes are reconstructed, Eq. 3b may be applied, in which  $[\text{NO}_3^-]$  is substituted for  $[\text{PO}_4^{3-}]$  in a 1:8 ratio. However, unless there are clear changes in the nutrient regime or sufficient proxy constraints on the nutrient concentrations, we prefer a calibration based exclusively on carbon isotope fractionation and carbonate system parameters, including sea surface temperature to calculate  $\delta^{13}\text{C}_{\text{CO}_2}$  from  $\delta^{13}\text{C}_{\text{DIC}}$ , to reconstruct  $p\text{CO}_2$ .

#### 4.4 Influence of carbon concentrating mechanisms: $\text{CO}_2$ insensitivity

As many phototrophs, including dinoflagellates, have mechanisms for concentrating  $\text{CO}_2$  near the cell membrane, the sensitivity of carbon isotope fractionation to ambient  $\text{CO}_2$  is expected to diminish below a certain concentration (M.R. Badger, 2003, M.P.S. Badger, 2021; Stoll et al., 2019). This is particularly the case as dinoflagellates utilize type II RubisCO, which has generally poorer performance compared to type I RubisCO at low  $\text{CO}_2$  concentrations (Giordano et al., 2005). Indeed, substantial activity of the carboxyl anhydrase (CA) enzyme, which facilitates the conversion of  $\text{HCO}_3^-$  to  $\text{CO}_2$  inside the cell or near the membrane, was observed in numerous dinoflagellate species, including *Lingulodinium* (Lapointe et al., 2008), *Symbiodinium* (Leggat et al., 1999) and the here analysed *Operculodinium* (Ratti et al., 2007). Also here we find a relatively low sensitivity at the lower end of the  $\text{CO}_2$  scale. The lower  $\text{CO}_2$  values correspond to the northern-most locations, with trends below  $240 \mu\text{atm}$  becoming somewhat obscured, at a minimum  $\epsilon_p\text{-CO}_2$  around 13 ‰ (Fig. 3). However, part of this levelling of the proxy-relationship may reflect the locally higher nutrient concentrations offsetting the higher  $\text{CO}_2$ . Though growth rates have a clear influence on  $\epsilon_p$  in algal groups (Burkhardt et al., 1999), including dinoflagellates (Wilkes et al., 2017), the dilute batch culturing experiments conducted with *P. reticulatum* showed no clear influence of growth rates on  $\epsilon_p$  (see also Sec. 4.2). It is also conceivable that higher growth rates influence  $\epsilon_p$  indirectly through, for example, seasonally enhanced  $\text{CO}_2$  drawdown, resulting in higher  $\delta^{13}\text{C}$  values in the remaining DIC. This effect may be enhanced by the relatively short growing season at the high latitudes. However, in culture experiments at low  $\text{CO}_2$  concentrations with other dinoflagellate species,  $^{13}\text{C}$ -fractionation was higher under nutrient limiting conditions than under replete conditions (Hoins et al., 2016b). Because of these confounding factors, the influence of carbon concentrating mechanisms on  $\epsilon_p$  in *O. centrocarpum* is difficult to gauge with the presently available data, and would ideally be tested using high nutrient or very low  $\text{CO}_2$  concentrations.

Still, also in the relatively limited range the current ocean offers for testing  $p\text{CO}_2$  proxies we have established a robust, albeit not overly sensitive, relation between  $p\text{CO}_2$  and dinocyst  $\delta^{13}\text{C}$ . Our cyst-based calibration yields more conservative and arguably more realistic absolute  $\text{CO}_2$  estimates and variability compared to available culture-based calibrations as it is based on the same compounds as will be analyzed in the paleo-domain. However, the low sensitivity at low  $\text{CO}_2$  implies that, until  
400 better constraints become available, the proposed calibration is potentially less suitable for application across, for example, the Pleistocene glacial periods. Further, it is important to realise that the value of  $240 \mu\text{atm}$  is based on the assumption that the  $\epsilon_p\text{-CO}_2 - p\text{CO}_2$  relation originated from cysts that have not been affected by the Suess-effect and thus represent a lower limit for  $\text{CO}_2$  (in)sensitivity. While our data does not preclude fractionation smaller than the here observed minimum ( $\sim 13 \text{‰}$ ) during low  $p\text{CO}_2$  periods, increased sensitivity at higher  $\text{CO}_2$  suggests that  $\text{CO}_2$  above (minimum)  $240 \mu\text{atm}$  and  $\text{CO}_2$  variability can  
405 be reconstructed with reasonable precision.

## 5. Conclusions - Proxy potential, limitations and calibrations

Our new modern ocean single-species carbon isotope fractionation dataset shows promising trends with environmental variables,  $p\text{CO}_2$  and nutrients. The selection of individual cysts allows control of cell size and species, which reduces  
410 uncertainty in proxy calibration and application compared to approaches based on organic substrates which inevitably integrate entire communities. Still, many of the challenges associated with other proxies based on organic substrates are encountered here as well. For example, we observed an impact of nutrients on carbon isotope fractionation, likely related to differences in growth rates. Similarly, at low  $p\text{CO}_2$  values sensitivity is reduced, possibly as a result of carbon concentrating mechanisms involved in dinoflagellate C uptake. Another remaining challenge is the observed difference between the cultured populations  
415 and cysts from the core top sediments. This is a pronounced difference, not only in the absolute isotope fractionation values but also in the slope of the  $\text{CO}_2$  sensitivity, which appears to be much larger for the cysts and requires attention in future culture studies.

The offset in  $\delta^{13}\text{C}$ , combined with uncertainties in fractionation between the motile cells and dinocysts imply that  $\text{CO}_2$  reconstructions using culture-based calibrations are more likely to overestimate past  $p\text{CO}_2$ . Furthermore, the large spread in  
420 our data ( $\sim 5 \text{‰}$  between high and low  $\text{CO}_2$ ) suggests that, due to this high sensitivity in the cysts, the method is also suited to study population dynamics.

### Data availability

All newly generated data will be available via a permanent online repository (Mendeley data doi: 10.17632/z6285myxkm.1)  
425 upon publication.

### Author contribution

AS & GJR designed the study, LvR, IK & JF processed samples, generated and analysed data, JF wrote the original draft, AS & GJR reviewed and edited the manuscript. AS acquired funding for this study.

430

### **Competing interests**

The authors declare that they have no conflict of interest.

### **Acknowledgments**

435 We thank A. van Dijk, M. Kienhuis and H. de Waard (Utrecht University) for technical and analytical assistance. AS acknowledges funding from Netherlands Organisation for Scientific Research (NWO) #ALWOP.223 and European Research Council (ERC) Starting grant #259627. This work was carried out under the program of the Netherlands Earth System Science Centre (NESSC), financially supported by the Dutch Ministry of Education, Culture and Science. We thank two anonymous reviewers for their insightful and highly constructive comments.

440

### **References**

- Anderson, D. M., Glibert, P. M. and Burkholder, J. M.: Harmful algal blooms and eutrophication: Nutrient sources, composition, and consequences, *Estuaries*, 25(4), 704–726, doi:10.1007/BF02804901, 2002.
- Badger, M.: The roles of carbonic anhydrases in photosynthetic CO<sub>2</sub> concentrating mechanisms, *Photosynth. Res.*, 77(2–3), 83–94, doi:10.1023/A:1025821717773, 2003.
- Badger, M. P. S.: Alkenone isotopes show evidence of active carbon concentrating mechanisms in coccolithophores as aqueous carbon dioxide concentrations fall below 7  $\mu\text{molL}^{-1}$ , *Biogeosciences*, 18(3), 1149–1160, doi:10.5194/bg-18-1149-2021, 2021.
- Barnola, J. M., Raynaud, D., Korotkevich, Y. S. and Lorius, C.: Vostok ice core provides 160,000-year record of atmospheric CO<sub>2</sub>, *Nature*, 329(6138), 408–414, doi:10.1038/329408a0, 1987.
- 450 Bijl, P. K., Houben, A. J. P., Schouten, S., Bohaty, S. M., Sluijs, A., Reichert, G.-J., Damsté, J. S. S. and Brinkhuis, H.: Transient Middle Eocene Atmospheric CO<sub>2</sub> and Temperature Variations, *Science* (80-. ), 330(6005), 819–821, doi:10.1126/science.1193654, 2010.
- Boller, A. J., Thomas, P. J., Cavanaugh, C. M. and Scott, K. M.: Low stable carbon isotope fractionation by coccolithophore RubisCO, *Geochim. Cosmochim. Acta*, 75(22), 7200–7207, doi:10.1016/j.gca.2011.08.031, 2011.
- 455 Boller, A. J., Thomas, P. J., Cavanaugh, C. M. and Scott, K. M.: Isotopic discrimination and kinetic parameters of RubisCO from the marine bloom-forming diatom, *Skeletonema costatum*, *Geobiology*, 13(1), 33–43, doi:10.1111/gbi.12112, 2015.
- Brandenburg, K. M., Rost, B., Van De Waal, D. B., Hoins, M. and Sluijs, A.: Physiological control on carbon isotope fractionation in marine phytoplankton, *Biogeosciences*, 19(13), 3305–3315, doi:10.5194/bg-19-3305-2022, 2022.
- Brinkhuis, H., Sengers, S., Sluijs, A., Warnaar, J., Williams, G. L. and Exon, N. F.: Latest Cretaceous-Earliest Oligocene and 460 Quaternary Dinoflagellate Cysts, ODP Site 1172, East Tasman Plateau, Proc. Ocean Drill. Program, Sci. results, 189(October), 48, 2003.

- Burkhardt, S., Riesebell, U. and Zondervan, I.: Effects of growth rate, CO<sub>2</sub> concentration, and cell size on the stable carbon isotope fractionation in marine phytoplankton, *Geochim. Cosmochim. Acta*, 63(22), 3729–3741, 1999.
- 465 Eberlein, T., Van de Waal, D., Brandenburg, K., John, U., Voss, M., Achterberg, E. and Rost, B.: Interactive effects of ocean acidification and nitrogen limitation on two bloom-forming dinoflagellate species, *Mar. Ecol. Prog. Ser.*, 543, 127–140, doi:10.3354/meps11568, 2016.
- Evitt, W. R.: Sporopollenin dinoflagellate cysts: their morphology and interpretation, *Amer Assn of Stratigraphic.*, 1985.
- Farquhar, G. D., Ehleringer, J. R. and Hubick, K. T.: *Discrimination and Photosynthesis*, 1989.
- 470 Fensome, R. A., MacRae, R. A., Moldowan, J. M., Taylor, F. J. R. and Williams, G. L.: The early Mesozoic radiation of dinoflagellates, *Paleobiology*, 329–338, 1996.
- Francey, R. J., Allison, C. E., Etheridge, D. M., Trudinger, C. M., Enting, I. G., Leuenberger, M., Langenfelds, R. L., Michel, E. and Steele, L. P.: A 1000-year high precision record of  $\delta^{13}\text{C}$  in atmospheric CO<sub>2</sub>, *Tellus, Ser. B Chem. Phys. Meteorol.*, 51(2), 170–193, doi:10.1034/j.1600-0889.1999.t01-1-00005.x, 1999.
- 475 Freeman, K. H.: Isotopic biogeochemistry of marine organic carbon, *Rev. Mineral. Geochemistry*, 43, 579–605, doi:10.2138/gsrng.43.1.579, 2001.
- Freeman, K. H. and Hayes, J. M.: Fractionation of carbon isotopes by phytoplankton and estimates of ancient CO<sub>2</sub> levels, *Global Biogeochem. Cycles*, 6(2), 185–198, 1992.
- Frieling, J. and Sluijs, A.: Towards quantitative environmental reconstructions from ancient non-analogue microfossil assemblages: Ecological preferences of Paleocene – Eocene dinoflagellates, *Earth-Science Rev.*, 185(August), 956–973, doi:10.1016/j.earscirev.2018.08.014, 2018.
- 480 Gattuso, J. P., Epitalon, J. M., Lavigne, H. and Orr, J.: seacarb: Seawater carbonate chemistry. R package version 3.2. 12., n.d.
- Giordano, M., Beardall, J. and Raven, J. A.: CO<sub>2</sub> Concentrating Mechanisms in Algae: Mechanisms, Environmental Modulation, and Evolution, *Annu. Rev. Plant Biol.*, 56(1), 99–131, doi:10.1146/annurev.arplant.56.032604.144052, 2005.
- 485 Goericke, R. and Fry, B.: Variations of marine plankton  $\delta^{13}\text{C}$  with latitude, temperature, and dissolved CO<sub>2</sub> in the world ocean, *Global Biogeochem. Cycles*, 8(1), 85–90, doi:10.1029/93GB03272, 1994.
- Gouretski, V. V. and Koltermann, K. P.: WOCE Global Hydrographic Climatology, *Berichte des Bundesamtes für Seeschiffahrt und Hydrogr.*, doi:10.5065/GS51-V170, 2004.
- Hallegraeff, G. M.: A review of harmful algal blooms and their apparent global increase\*, *Phycologia*, 32(2), 79–99, doi:10.2216/i0031-8884-32-2-79.1, 1993.
- 490 Hayes, J. M.: Fractionation of Carbon and Hydrogen Isotopes in Biosynthetic Processes, *Rev. Mineral. Geochemistry*, 43(1), 225–277, doi:10.2138/gsrng.43.1.225, 2001.
- Hayes, J. M., Strauss, H. and Kaufman, A. J.: The abundance of <sup>13</sup>C in marine organic matter and isotopic fractionation in the global biogeochemical cycle of carbon during the past 800 Ma, *Chem. Geol.*, 161(1), 103–125, 1999.
- Head, M. J.: Modern dinoflagellate cysts and their biological affinities, *Palynol. Princ. Appl.*, 3, 1197–1248, 1996.
- 495 Henderiks, J. and Pagani, M.: Refining ancient carbon dioxide estimates: Significance of coccolithophore cell size for

- alkenone-based p CO<sub>2</sub> records, *Paleoceanography*, 22(3), n/a-n/a, doi:10.1029/2006PA001399, 2007.
- Hoins, M., Van de Waal, D. B., Eberlein, T., Reichart, G.-J., Rost, B. and Sluijs, A.: Stable carbon isotope fractionation of organic cyst-forming dinoflagellates: Evaluating the potential for a CO<sub>2</sub> proxy, *Geochim. Cosmochim. Acta*, 160, 267–276, doi:10.1016/j.gca.2015.04.001, 2015.
- 500 Hoins, M., Eberlein, T., Van de Waal, D. B., Sluijs, A., Reichart, G.-J. and Rost, B.: CO<sub>2</sub>-dependent carbon isotope fractionation in dinoflagellates relates to their inorganic carbon fluxes, *J. Exp. Mar. Bio. Ecol.*, 481, 9–14, doi:10.1016/j.jembe.2016.04.001, 2016a.
- Hoins, M., Eberlein, T., Großmann, C. H., Brandenburg, K., Reichart, G.-J., Rost, B., Sluijs, A. and Van de Waal, D. B.: Combined Effects of Ocean Acidification and Light or Nitrogen Availabilities on <sup>13</sup>C Fractionation in Marine Dinoflagellates, *PLoS One*, 11(5), e0154370, doi:10.1371/journal.pone.0154370, 2016b.
- 505 IPCC: Climate Change 2014: Synthesis Report. Contribution of Working Groups I, II and III to the Fifth Assessment Report of the Intergovernmental Panel on Climate Change, 2014.
- Keeling, R. F., Graven, H. D., Welp, L. R., Resplandy, L., Bi, J., Piper, S. C., Sun, Y., Bollenbacher, A. and Meijer, H. A. J.: Atmospheric evidence for a global secular increase in carbon isotopic discrimination of land photosynthesis, *Proc. Natl. Acad. Sci. U. S. A.*, 114(39), 10361–10366, doi:10.1073/pnas.1619240114, 2017.
- 510 Kodrans-Nsiah, M., De Lange, G. J. and Zonneveld, K. A. F.: A natural exposure experiment on short-term species-selective aerobic degradation of dinoflagellate cysts, *Rev. Palaeobot. Palynol.*, 152(1), 32–39, 2008.
- Lapointe, M., MacKenzie, T. D. B. and Morse, D.: An external  $\delta$ -carbonic anhydrase in a free-living marine dinoflagellate may circumvent diffusion-limited carbon acquisition, *Plant Physiol.*, 147(3), 1427–1436, doi:10.1104/pp.108.117077, 2008.
- 515 de Leeuw, J. W., Versteegh, G. J. M. and van Bergen, P. F.: Biomacromolecules of Algae and Plants and their Fossil Analogues, *Plant Ecol.*, 182(1–2), 209–233, doi:10.1007/s11258-005-9027-x, 2006.
- Leggat, W., Badger, M. R. and Yellowlees, D.: Evidence for an inorganic carbon-concentrating mechanism in the symbiotic dinoflagellate *Symbiodinium* sp., *Plant Physiol.*, 121(4), 1247–1255, doi:10.1104/pp.121.4.1247, 1999.
- Magozzi, S., Yool, A., Vander Zanden, H. B., Wunder, M. B. and Trueman, C. N.: Using ocean models to predict spatial and temporal variation in marine carbon isotopes, *Ecosphere*, 8(5), e01763, doi:10.1002/ecs2.1763, 2017.
- 520 Mertens, K. N., Ribeiro, S., Bouimetarhan, I., Caner, H., Combourieu Nebout, N., Dale, B., De Vernal, A., Ellegaard, M., Filipova, M., Godhe, A., Goubert, E., Grøsfjeld, K., Holzwarth, U., Kotthoff, U., Leroy, S. A. G., Londeix, L., Marret, F., Matsuoka, K., Mudie, P. J., Naudts, L., Peña-Manjarrez, J. L., Persson, A., Popescu, S. M., Pospelova, V., Sangiorgi, F., van der Meer, M. T. J., Vink, A., Zonneveld, K. A. F., Vercauteren, D., Vlassenbroeck, J., Louwey, S., Nebout, N. C., Dale, B.,
- 525 De Vernal, A., Ellegaard, M., Filipova, M. and Godhe, A.: Process length variation in cysts of a dinoflagellate, *Lingulodinium machaerophorum*, in surface sediments: investigating its potential as salinity proxy, *Mar. Micropaleontol.*, 70(1), 54–69, doi:10.1016/j.marmicro.2008.10.004, 2009.
- Mook, W. G., Bommerson, J. C. and Staverman, W. H.: Carbon isotope fractionation between dissolved bicarbonate and gaseous carbon dioxide, *Earth Planet. Sci. Lett.*, 22(2), 169–176, doi:10.1016/0012-821X(74)90078-8, 1974.



- 530 Naafs, B. D. A., Castro, J. M., De Gea, G. A., Quijano, M. L., Schmidt, D. N. and Pancost, R. D.: Gradual and sustained carbon dioxide release during Aptian Oceanic Anoxic Event 1a, *Nat. Geosci.*, 9(2), 135–139, doi:10.1038/ngeo2627, 2016.
- Nooteboom, P. D., Bijl, P. K., van Sebille, E., von der Heydt, A. S. and Dijkstra, H. A.: Transport bias by ocean currents in sedimentary microplankton assemblages: Implications for paleoceanographic reconstructions, *Paleoceanogr. Paleoclimatology*, doi:10.1029/2019PA003606, 2019.
- 535 Pagani, M.: *Biomarker-Based Inferences of Past Climate: The Alkenone pCO<sub>2</sub> Proxy*, 2nd ed., Elsevier Ltd., 2013.
- Pagani, M., Liu, Z., LaRiviere, J. and Ravelo, A. C.: High Earth-system climate sensitivity determined from Pliocene carbon dioxide concentrations, *Nat. Geosci.*, 3(1), 27–30, doi:10.1038/ngeo724, 2010.
- Pagani, M., Huber, M., Liu, Z., Bohaty, S. M., Henderiks, J., Sijp, W. P., Krishnan, S. and DeConto, R. M.: The Role of Carbon Dioxide During the Onset of Antarctic Glaciation, *Science* (80-. ), 334, 1261–1265, doi:10.1126/science.1203909,
- 540 2011.
- PALAEOSENS: Making sense of palaeoclimate sensitivity, *Nature*, 491(7426), 683–691, doi:10.1038/nature11574, 2012.
- Pancost, R. D. and Pagani, M.: Controls on the carbon isotopic compositions of lipids in marine environments, *Handb. Environ. Chem. Vol. 2 React. Process.*, 2 N(October 2005), 209–249, doi:10.1007/698\_2\_007, 2006.
- Popp, B. N., Laws, E. A., Bidigare, R. R., Dore, J. E., Hanson, K. L. and Wakeham, S. G.: Effect of Phytoplankton Cell
- 545 Geometry on Carbon Isotopic Fractionation, *Geochim. Cosmochim. Acta*, 62(1), 69–77, doi:10.1016/S0016-7037(97)00333-5, 1998.
- Rae, J. W. B., Zhang, Y. G., Liu, X., Foster, G. L., Stoll, H. M. and Whiteford, R. D. M.: Atmospheric CO<sub>2</sub> over the Past 66 Million Years from Marine Archives , *Annu. Rev. Earth Planet. Sci.*, 49(1), 599–631, doi:10.1146/annurev-earth-082420-063026, 2021.
- 550 Ratti, S., Giordano, M. and Morse, D.: CO<sub>2</sub>-concentrating mechanisms of the potentially toxic dinoflagellate *Protoceratium reticulatum* (Dinophyceae, Gonyaulacales), *J. Phycol.*, 43(4), 693–701, doi:10.1111/j.1529-8817.2007.00368.x, 2007.
- Roeske, C. A. and O’Leary, M. H.: Carbon isotope effects on enzyme-catalyzed carboxylation of ribulose biphosphate, *Biochemistry*, 23(25), 6275–6284, doi:10.1021/bi00320a058, 1984.
- van Roij, L., Sluijs, A., Laks, J. J. and Reichart, G.-J.: Stable carbon isotope analyses of ng quantities of particulate organic
- 555 carbon (pollen) with laser ablation nano combustion gas chromatography isotope ratio mass spectrometry, *Rapid Commun. Mass Spectrom.*, (October 2016), 47–58, doi:10.1002/rcm.7769, 2016.
- Rost, B., Richter, K.-U., Riesebell, U. and Hansen, P. J.: Inorganic carbon acquisition in red tide dinoflagellates, *Plant, Cell Environ.*, 29(5), 810–822, doi:10.1111/j.1365-3040.2005.01450.x, 2006.
- Schoon, P. L., Sluijs, A., Sinninghe Damsté, J. S. and Schouten, S.: Stable carbon isotope patterns of marine biomarker lipids
- 560 in the Arctic Ocean during Eocene Thermal Maximum 2, *Paleoceanography*, 26(3), doi:10.1029/2010PA002028, 2011.
- Schouten, S., Klein Breteler, W. C. ., Blokker, P., Schogt, N., Rijpstra, W. I. C., Grice, K., Baas, M. and Sinninghe Damsté, J. S.: Biosynthetic effects on the stable carbon isotopic compositions of algal lipids: implications for deciphering the carbon isotopic biomarker record, *Geochim. Cosmochim. Acta*, 62(8), 1397–1406, doi:10.1016/S0016-7037(98)00076-3, 1998.

- Sharkey, T. D. and Berry, J. A.: Carbon isotope fractionation of algae as influenced by an inducible CO<sub>2</sub> concentrating mechanism, in *Inorganic carbon uptake by Aquatic Photosynthetic organisms*, edited by W. J. Lucas and J. A. Berry, pp. 389–401, the American Society of Plant Physiologists., 1985.
- Sluijs, A., van Roij, L., Frieling, J., Laks, J. and Reichart, G.-J.: Single-species dinoflagellate cyst carbon isotope ecology across the Paleocene-Eocene Thermal Maximum, *Geology*, 46(1), 79–82, doi:10.1130/G39598.1, 2018.
- Stoll, H. M., Guitian, J., Hernandez-Almeida, I., Mejia, L. M., Phelps, S., Polissar, P., Rosenthal, Y., Zhang, H. and Ziveri, P.: Upregulation of phytoplankton carbon concentrating mechanisms during low CO<sub>2</sub> glacial periods and implications for the phytoplankton pCO<sub>2</sub> proxy, *Quat. Sci. Rev.*, 208, 1–20, doi:10.1016/j.quascirev.2019.01.012, 2019.
- Tagliabue, A. and Bopp, L.: Towards understanding global variability in ocean carbon-13, *Global Biogeochem. Cycles*, 22(1), 1–13, doi:10.1029/2007GB003037, 2008.
- Takahashi, T., Sutherland, S. C., Chipman, D. W., Goddard, J. G., Ho, C., Newberger, T., Sweeney, C. and Munro, D. R.: Climatological distributions of pH, pCO<sub>2</sub>, total CO<sub>2</sub>, alkalinity, and CaCO<sub>3</sub> saturation in the global surface ocean, and temporal changes at selected locations, *Mar. Chem.*, 164, 95–125, doi:10.1016/j.marchem.2014.06.004, 2014.
- Takahashi, T., Sutherland, S. C. and Kozyr, A.: *Global Ocean Surface Water Partial Pressure of CO<sub>2</sub> Database: Measurements Performed During 1957-2015 (Version 2015)*, Carbon Dioxide Information Analysis Center, Oak Ridge National Laboratory, U.S. Department of Energy, Oak Ridge, Tennessee., n.d.
- Versteegh, G. J. M., Blokker, P., Marshall, C. and Pross, J.: Macromolecular composition of the dinoflagellate cyst *Thalassiphora pelagica* (Oligocene, SW Germany), *Org. Geochem.*, 38(10), 1643–1656, doi:10.1016/j.orggeochem.2007.06.007, 2007.
- Versteegh, G. J. M., Blokker, P., Bogus, K., Harding, I. C., Lewis, J., Oltmanns, S., Rochon, A. and Zonneveld, K. A. F.: Infra red spectroscopy, flash pyrolysis, thermally assisted hydrolysis and methylation (THM) in the presence of tetramethylammonium hydroxide (TMAH) of cultured and sediment-derived *Lingulodinium polyedrum* (Dinoflagellata) cyst walls, *Org. Geochem.*, 43, 92–102, doi:10.1016/j.orggeochem.2011.10.007, 2012.
- Van de Waal, D. B., John, U., Ziveri, P., Reichart, G.-J., Hoins, M., Sluijs, A. and Rost, B.: Ocean Acidification Reduces Growth and Calcification in a Marine Dinoflagellate, *PLoS One*, 8(6), doi:10.1371/journal.pone.0065987, 2013.
- Wall, D. and Dale, B.: “Living fossils” in Western Atlantic plankton, *Nature*, 211(5053), 1025–1026 [online] Available from: <http://www.scopus.com/inward/record.url?eid=2-s2.0-0000259853&partnerID=40&md5=441e2fd50df53b93e4d31aa0ba9e6015>, 1966.
- Wilkes, E. B. and Pearson, A.: A general model for carbon isotopes in red-lineage phytoplankton: Interplay between unidirectional processes and fractionation by RubisCO, *Geochim. Cosmochim. Acta*, 265, 163–181, doi:10.1016/j.gca.2019.08.043, 2019.
- Wilkes, E. B., Carter, S. J. and Pearson, A.: CO<sub>2</sub>-dependent carbon isotope fractionation in the dinoflagellate *Alexandrium tamarense*, *Geochim. Cosmochim. Acta*, 212, 48–61, doi:10.1016/j.gca.2017.05.037, 2017.
- Wilkes, E. B., Lee, R. B. Y., McClelland, H. L. O., Rickaby, R. E. M. and Pearson, A.: Carbon isotope ratios of coccolith-

- associated polysaccharides of *Emiliana huxleyi* as a function of growth rate and CO<sub>2</sub> concentration, *Org. Geochem.*, 119, 1–10, doi:10.1016/j.orggeochem.2018.02.006, 2018.
- 600 Williams, G. L., Brinkhuis, H., Pearce, M. A., Fensome, R. A. and Weegink, J. W.: Southern Ocean and global dinoflagellate cyst events compared: index events for the Late Cretaceous–Neogene, in *Proceedings of the Ocean Drilling Program, Scientific Results*, vol. 189, pp. 1–98., 2004.
- Witkowski, C. R., Weijers, J. W. H., Blais, B., Schouten, S. and Sinninghe Damsté, J. S.: Molecular fossils from phytoplankton reveal secular P co<sub>2</sub> trend over the Phanerozoic, *Sci. Adv.*, 4(11), eaat4556, doi:10.1126/sciadv.aat4556, 2018.
- 605 Zhang, H., Torres-Romero, I. and Stoll, H. M.: Re-examining extreme carbon isotope fractionation in the coccolithophore *Ochrosphaera neapolitana*, *Nat. Commun.*, 13(1), 7606, doi:10.1038/s41467-022-35109-4, 2022.
- Zonneveld, K. A. F., Versteegh, G. J. M. and De Lange, G. J.: Preservation of organic-walled dinoflagellate cysts in different oxygen regimes: a 10,000 year natural experiment, *Mar. Micropaleontol.*, 29(3), 393–405, 1997.
- Zonneveld, K. A. F., Marret, F., Versteegh, G. J. M., Bogus, K., Bonnet, S., Bouimtarhan, I., Crouch, E., de Vernal, A.,
- 610 Elshanawany, R., Edwards, L., Esper, O., Forke, S., Grøsfjeld, K., Henry, M., Holzwarth, U., Kieft, J.-F., Kim, S.-Y., Ladouceur, S., Ledu, D., Chen, L., Limoges, A., Londeix, L., Lu, S.-H., Mahmoud, M. S., Marino, G., Matsouka, K., Matthiessen, J., Mildenhall, D. C., Mudie, P., Neil, H. L., Pospelova, V., Qi, Y., Radi, T., Richerol, T., Rochon, A., Sangiorgi, F., Solignac, S., Turon, J.-L., Verleye, T., Wang, Y., Wang, Z. and Young, M.: Atlas of modern dinoflagellate cyst distribution based on 2405 data points, *Rev. Palaeobot. Palynol.*, 191, 1–197, doi:10.1016/j.revpalbo.2012.08.003, 2013.
- 615 Zonneveld, K. A. F., Gray, D. D., Kuhn, G. and Versteegh, G. J. m.: Postdepositional aerobic and anaerobic particulate organic matter degradation succession reflected by dinoflagellate cysts: The Madeira Abyssal Plain revisited, *Mar. Geol.*, 408, 87–109, doi:10.1016/j.margeo.2018.11.010, 2019.

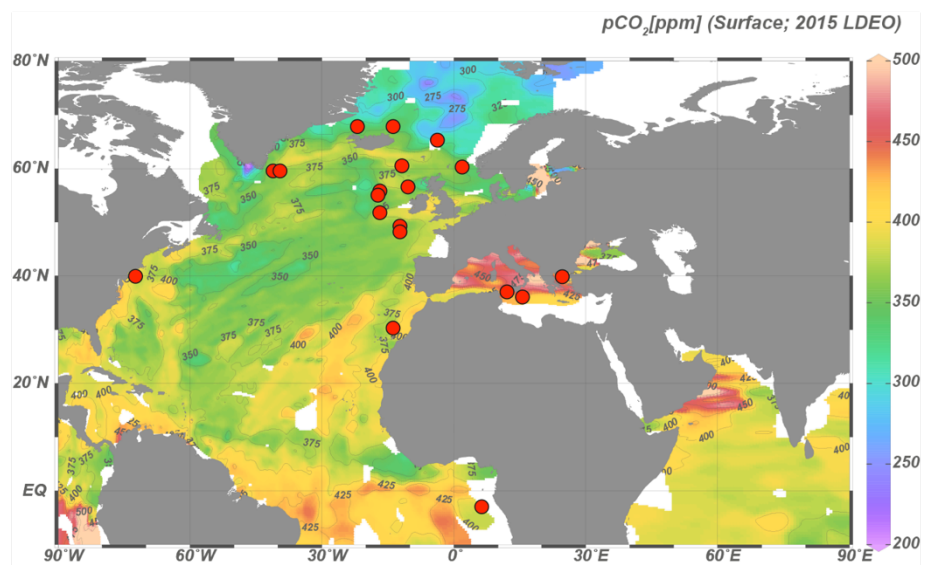
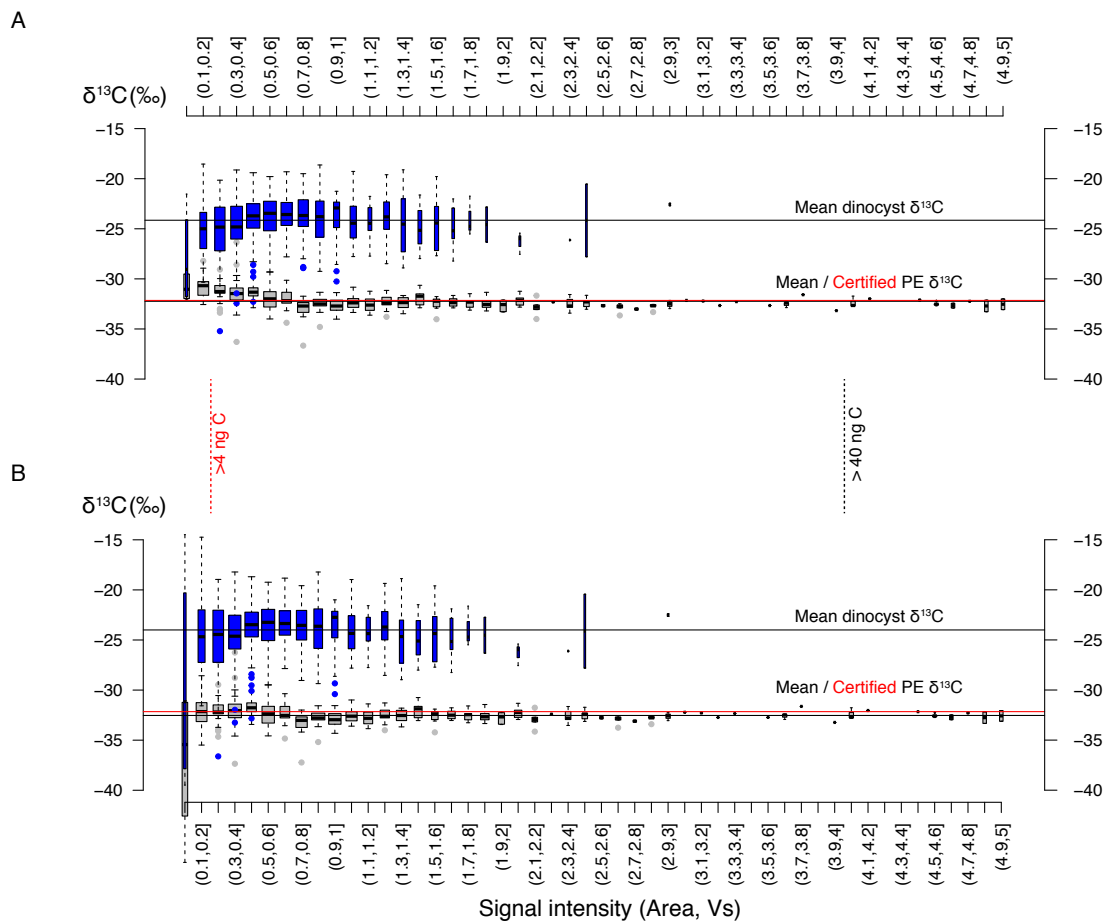


**Figure 1.** Locations of samples with sufficient *Operculodinium centrocarpum* and/or *Spiniferites* spp for dinoflagellate cyst  $\delta^{13}\text{C}$  analyses.



625 **Figure 2. Signal intensity in Volt seconds (Vs) versus carbon isotope value distribution within bins of 0.1 Vs. A.** The  
 630 blue boxplots represent our new dinocyst  $\delta^{13}\text{C}$ , and the gray boxplots represent the previously published data for the PE  
 standard ( $\delta^{13}\text{C}$  value  $-32.151\text{‰} \pm 0.050\text{‰}$ ;  $1\sigma$ ). **B.** Same as A. but for background-corrected values (see §3.2). The vertical  
 black and red line represent cut-off values for individual PE standard measurements (>4 Vs;  $\sim 42$  ng C; 0.5‰ precision) and  
 individual cyst measurements (>0.2 Vs;  $\sim 6$  ng C), respectively. The width of each boxplot is square-root scaled with the  
 number of measurements in the respective bins. Note that several bins at the high-end do not contain any data.



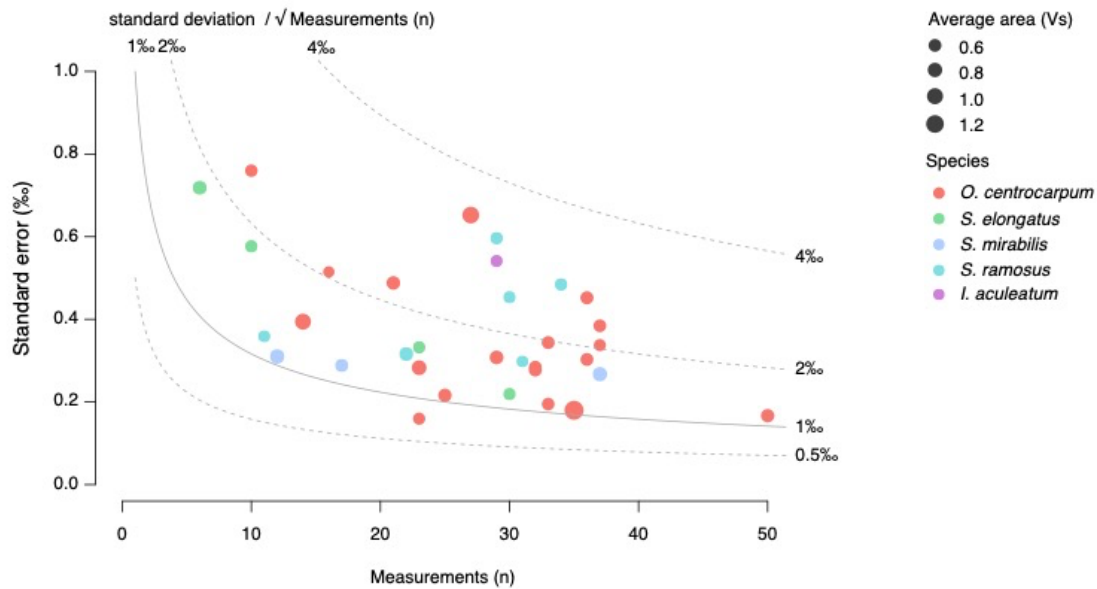
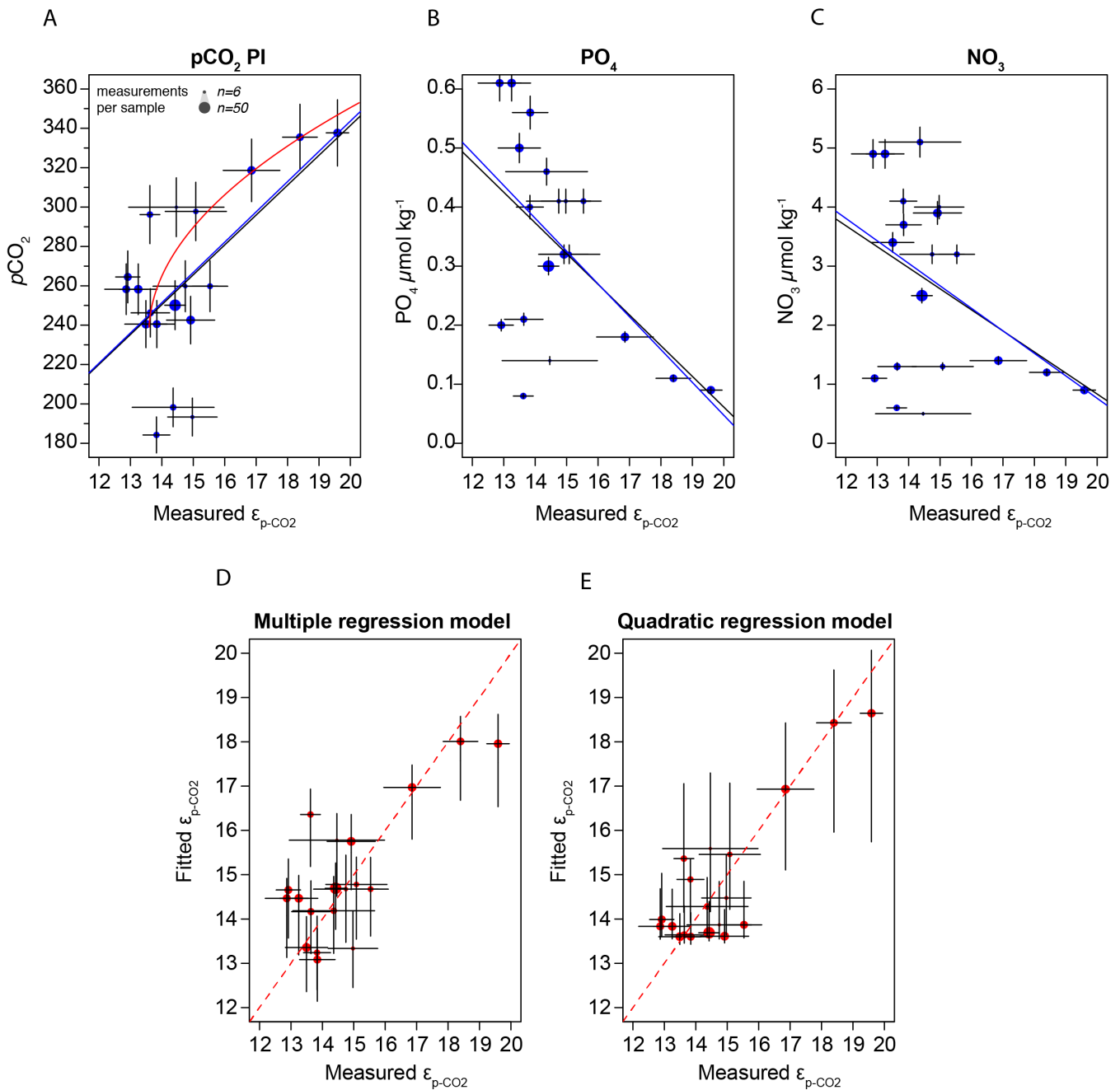


**Figure 4.** Relation of standard error of  $\delta^{13}\text{C}_{\text{DINO}}$  (‰) with the number of measurements and signal intensity (area in Volt seconds (Vs)). Colors correspond to the various analyzed species.



640

**Figure 5.** Regression analyses for  $\epsilon_{p\text{-CO}_2}$  of *O. centrocarpum* relative to (a)  $p\text{CO}_2$  (measured, corrected to pre-industrial values); black line represents simple linear regression, blue lines represent weighted linear regressions and red line (a) represents weighted quadratic regression, (b) phosphate concentrations ( $\text{PO}_4^{3-}$ ), (c) nitrate concentrations ( $\text{NO}_3^-$ ). (d) Fitted values illustrating the multiple regression model performance using parameters a-c relative to measured  $\epsilon_{p\text{-CO}_2}$ . (e) Fitted values using

645

only pre-industrial  $p\text{CO}_2$  but applying a quadratic regression (red curve in panel a). Errors in panels a-c represent 5% of the



measured value and errors on the fitted values in panels d and e represent propagated errors of both measurements and environmental variables (as shown in panel a-c) using Monte-Carlo simulations ( $n=1000$ ) for regression models. Symbol size (top left corner of panel a) represents the number of measurements within each sample.

Core-ID	Latitude (°N)	Longitude (°E)	Species	Measurements (n)	S-W normality
NF2012-091	37.977402	-73.669403	<i>O.centrocarpum</i>	22 (21)	* ()
PE360-24	55.496231	-15.800755	<i>O.centrocarpum</i>	24 (23)	** ()
PE360-45	55.539398	-15.8453	<i>O.centrocarpum</i>	23 (16)	()
NA87-02	64.480003	-5.83	<i>O.centrocarpum</i>	20 (14)	*** ()
LCD13	67.501282	-15.069252	<i>O.centrocarpum</i>	25 (25)	()
LCD10A	66.677437	-24.179598	<i>O.centrocarpum</i>	29 (27)	()
MedSea (MC-613)	35.8575	14.105556	<i>O.centrocarpum</i>	35 (35)	()
MedSea (MC-614)	35.8075	12.998056	<i>O.centrocarpum</i>	33 (32)	* ()
MedSea (MC-645)	40.2175	25.244167	<i>O.centrocarpum</i>	33 (23)	** ()
ENAM93-08bx	59.501667	3.69	<i>O.centrocarpum</i>	38 (37)	*()
			<i>S.ramosus</i>	33 (32)	()
ENAM94-13bx	60.249997	-11.19	<i>O.centrocarpum</i>	36 (33)	()
			<i>S.elongatus</i>	34 (30)	*** ()
			<i>S.mirabilis</i>	13 (12)	()
ENAM96-09bx	57.159917	-10.26	<i>O.centrocarpum</i>	39 (37)	()
			<i>S.ramosus</i>	30 (29)	()
ENAM97-04	52.410386	-14.94	<i>O.centrocarpum</i>	52 (50)	()
			<i>S.elongatus</i>	23 (23)	()
			<i>S.mirabilis</i>	38 (37)	** (*)
Omex93-A2 bx	49.483	-11.13	<i>O.centrocarpum</i>	30 (29)	()
			<i>S.ramosus</i>	13 (11)	*()
			<i>S.elongatus</i>	6 (6)	()
			<i>S.mirabilis</i>	18 (17)	()
PE275-6	59.272369	-38.36	<i>O.centrocarpum</i>	34 (33)	*()
			<i>S.ramosus</i>	34 (30)	**()
PE275-9	59.272369	-38.36	<i>O.centrocarpum</i>	37 (36)	*(*)
			<i>S.ramosus</i>	23 (22)	*(*)
			<i>S.elongatus</i>	12 (10)	*(*)
T89-15bx	-4.199372	10.05	<i>O.centrocarpum</i>	36 (36)	* (*)
			<i>S.ramosus</i>	35 (34)	* (*)
64PE428-1-1-6	47.079782	-10.197305	<i>O.centrocarpum</i>	35 (33)	()
			<i>I.aculeatum</i>	30 (29)	()
64PE428-1-6-6	30.67917	-11.930478	<i>O.centrocarpum</i>	11 (10)	()

**Table 1. Core localities, analyzed species, number of measurements and normality of the carbon isotope data.** Number of measurements total and in parentheses measurements used for environmental comparisons (see also results §3.4). Shapiro-

655 Wilk (S-W) normality test on data: non-normal data distributions are indicated where  $p$  values are  $< 0.1$  (\*),  $< 0.01$  (\*\*) and  $< 0.001$  (\*\*\*), in parentheses the same for the data used for environmental comparisons.

**Table 2a:** Linear regression coefficients and significance for all samples where *O. centrocarpum* was analyzed (n = 19), with  $\varepsilon_{p-CO_2}$  as dependent variable. Parameters with p-values <0.05 in bold.

	Coeff.	Std.err.	t	p	R <sup>2</sup>
CO <sub>2</sub> (mol/kg)	-2.506e+05	5.603e+05	-0.447	0.66039	0.01163
CO <sub>3</sub> <sup>2-</sup> (mol/kg)	41263.663	15432.856	2.674	0.0160	0.296
HCO <sub>3</sub> <sup>-</sup> (mol/kg)	809.88	7057.32	0.115	0.910	0.0007741
DIC(mol/kg)	5655.859	6266.998	0.902	0.379	0.04572
SST (°C)	0.16971	0.06043	2.809	0.0121	0.3169
SSS (psu)	0.6737	0.3604	1.869	0.0789	0.1705
PO <sub>4</sub> <sup>3-</sup> (μmol /kg)	-5.5131	2.1102	-2.613	0.0182	0.2865
NO <sub>3</sub> <sup>-</sup> (μmol /kg)	-0.4484	0.2493	-1.798	0.0899	0.1599
Si (μmol /kg)	-0.2553	0.3298	-0.774	0.449	0.03405
O <sub>2</sub> (mL/L)	-1.274	0.433	-2.943	0.0091	0.3375
ALK (mol/kg)	7621.253	4712.178	1.617	0.124	0.1334
pCO <sub>2</sub> ~1850	0.024945	0.007752	3.218	0.005050	0.3785

660

**Table 2b:** As Table 2a, but with  $\varepsilon_{p-DIC}$  as dependent variable.

	Coeff.	Std.err.	t	p	R <sup>2</sup>
CO <sub>2</sub> (mol/kg)	1.133e+05	4.760e+05	0.238	0.815	0.00332
CO <sub>3</sub> <sup>2-</sup> (mol/kg)	19589.987	14818.493	1.322	0.204	0.09322
HCO <sub>3</sub> <sup>-</sup> (mol/kg)	6547.21	5758.02	1.137	0.271	0.07068
DIC(mol/kg)	7803.835	5086.841	1.534	0.143	0.1216
SST (°C)	0.04959	0.06068	0.817	0.425	0.03781
SSS (psu)	0.4043	0.3201	1.263	0.224	0.08579
PO <sub>4</sub> <sup>3-</sup> (μmol /kg)	-2.3993	2.0318	-1.181	0.254	0.07581
NO <sub>3</sub> <sup>-</sup> (μmol /kg)	-0.05666	0.22969	-0.247	0.808	0.003567
Si (μmol /kg)	-0.01925	0.28388	-0.068	0.947	0.0002703
O <sub>2</sub> (mL/L)	-0.4170	0.4385	-0.951	0.355	0.05051
ALK (mol/kg)	6754.843	3956.586	1.707	0.106	0.1464
pCO <sub>2</sub> ~1850	0.010083	0.007952	1.268	0.222	0.0864